

Using t-SNE for characterizing glitches in LIGO detectors

Tabata Aira Ferreira, Gabriela González

Louisiana State University, Baton Rouge, LA 70803, USA

E-mail: tferreira@lsu.edu

Abstract. Glitches are non-Gaussian noise transients originating from environmental and instrumental sources that contaminate data from gravitational wave detectors. Some glitches can even mimic gravitational wave signals from compact object mergers, which are the primary targets of terrestrial observatories. In this study, we present a method to analyze noise transients from the LIGO observatories using Q-transform information combined with t-Distributed Stochastic Neighbor Embedding (t-SNE). We implement classification techniques, examine the influence of parameters on glitch classification, and conduct a week-long daily analysis to track outlier transients over time.

1. Introduction

From September 14 2015, to the recent first part of the fourth observing run, O4a, around 170 gravitational wave signals from mergers of compact objects such as neutron stars and black holes have been detected [1–4]. The LVK collaboration, consisting of LIGO (Laser Interferometer Gravitational-Wave Observatory) [5–7], Virgo [8], and KAGRA [9–11], is actively engaged in the search for new more detections and further knowledge about the Universe; achievements that involve researchers from different fields including data analysis, computer science, instrumental, and experimental groups worldwide. Each aspect of these areas is crucial.

The observatories are constantly being modified to achieve the best possible sensitivity through experimental tests and instrumental changes. However, with increased sensitivity, they also become more susceptible to *glitches*, non-Gaussian noise transients, that have the potential to contaminate gravitational wave data. Glitches are usually associated with environmental or instrumental sources; during the third observing run (O3), for instance, LIGO was significantly affected by glitches from light scattering [12, 13], which contaminated the data mainly between 20 and 40 Hz during high-ground motions.

In general, these noise transients pollute the data, affecting the search for gravitational waves, increasing the background noise in the statistical analysis, and

making difficult the search for *burst* signals, which are short in duration, unmodeled, and originated from events such as core-collapse supernovae [14]. Some glitches may resemble real signals, potentially leading to false positives, while others may coincide with actual gravitational wave signals, as occurred during the first detection of a binary neutron star merger, GW170817 [15].

Glitches are typically visualized via spectrograms, from which we can derive characteristics such as frequencies, duration, morphology, and signal-to-noise ratio (SNR). The study of glitches is one of the responsibilities of the Detector Characterization (DetChar) group. To identify glitch sources, Detchar frequently relies on auxiliary channels, which record data from sensors distributed throughout the interferometers [16, 17]. These sensors include photodiodes, magnetometers, seismometers, thermometers, microphones, and others. Temporal (and sometimes morphological) coincidences between these sensors and the gravitational wave channel, where LIGO stores information about potential gravitational wave candidates, can help indicate the source of glitches. Additionally, such coincidences assist in validating gravitational wave events [16, 18].

Understanding the behavior of glitches is crucial for identifying their sources and hopefully eliminating or reducing their occurrences. LIGO looks for glitches by using *Omicron*, a tool that performs a multi-resolution analysis of gravitational data in the time-frequency domain [19, 20]. *Omicron* processes the data via the Q-transform [21] in two stages. First, it analyzes transients across different time-frequency planes (also known as Q-planes), which vary according to a quality factor parameter, Q . This information is typically stored in what we will refer to as “unclustered files”. Subsequently, after clustering over time, *Omicron* stores information for each glitch with representative parameters such as frequency, duration, signal-to-noise ratio (SNR), and others. From clustered *Omicron* information, tools like *Gravity Spy* [22–24] are able to classify glitches by analyzing their morphologies in spectrograms.

This paper presents a method for characterizing glitches using *t*-SNE, *t*-Distributed Stochastic Neighbor Embedding, on unclustered *Omicron* data. We provide examples of the method’s application to O3b, the second half of the third LIGO observing run, and explore an example of its use during O4a. Since *Omicron* already runs daily, there is no need to generate new spectrograms or new data for this analysis. Additionally, this method does not require the creation of a training dataset and can analyze glitches with low latency (within a few minutes) as it relies solely on *Omicron*.

Section 2 provides an overview of transient noise features, examines how *Omicron* unclustered data vary with Q -values, outlines the main classes of glitches, and introduces the method using the *t*-SNE algorithm. Section 3 discusses the O3b LIGO Livingston application and explores how parameter selection affects the results, using *Gravity Spy* classifications as a reference. Section 4 presents results obtained without prior knowledge of glitch classes. The same approach is shown in Section 5, where outliers during O4a are identified and tracked over time, also without prior class knowledge. Finally, Section 6 summarizes the conclusions and discusses perspectives for future work.

2. Transient Noise

Transient noise, or glitches, create an excess background for astrophysical signals. To identify the presence of these unwanted signals, LIGO uses a tool called Omicron to detect excess power in the main gravitational wave data channel. It then applies a Q-transform to characterize these glitches based on their frequency, time, SNR, and Q-value, Q . The Q-value is related to the bisquare window in the Q-transform and proportional to the frequency window f_0 , and its bandwidth Δf_0 [25],

$$Q \propto \frac{f_0}{\Delta f_0}. \quad (1)$$

The primary advantage of using the Q-transform lies in its ability to vary the resolution in both time and frequency within a time-frequency representation. In the initial stage, Omicron saves the transient information in unclustered files (in ROOT format) [26], which includes storing parameters for all *tiles* across various Q-values. In the context of spectrogram generation via the Q-transform, a *tile* is defined as a rectangle with a height of Δf_0 and a width of Δt , built for different Q-values. The second step involves time clustering, where a single representative data point is selected for each transient. Figure 1 presents a *glitchgram*, which is a time and frequency representation of glitches from clustered files over the period of a day. Information stored in the glitchgrams is crucial for understanding glitch behavior across different periods. On the day in Figure 1, there are significant broadband glitches between 20 and 40 Hz with low SNR, as indicated by the color of the data points.

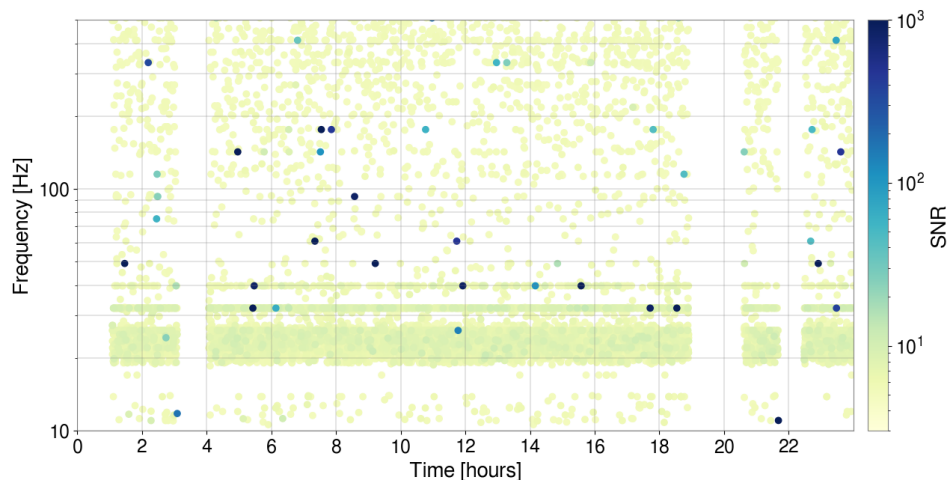


Figure 1: A one-day glitchgram during O4a at LHO (LIGO Hanford Observatory), built from Omicron clustered files. Each glitch is represented by a data point showing its frequency, time of occurrence, and SNR.

For each one of these glitches, we can access the ROOT files to get the unclustered information. Figure 2 illustrates the time-frequency distribution of unclustered triggers‡

‡ Here, we refer to each data point from unclustered Omicron as a trigger.

across various Q-planes for one of the most common glitches observed during O4a at the LIGO Livingston Observatory (LLO). Blue indicates SNR below 10, red indicates SNR above 20, and green indicates SNR values in between. The parameter Q, from Equation 1, can be interpreted as follows: a higher Q-value results in higher resolution in frequency, while a lower Q-value results in worse resolution in frequency (or better resolution in time [27]). This characteristic is observable when comparing the images.

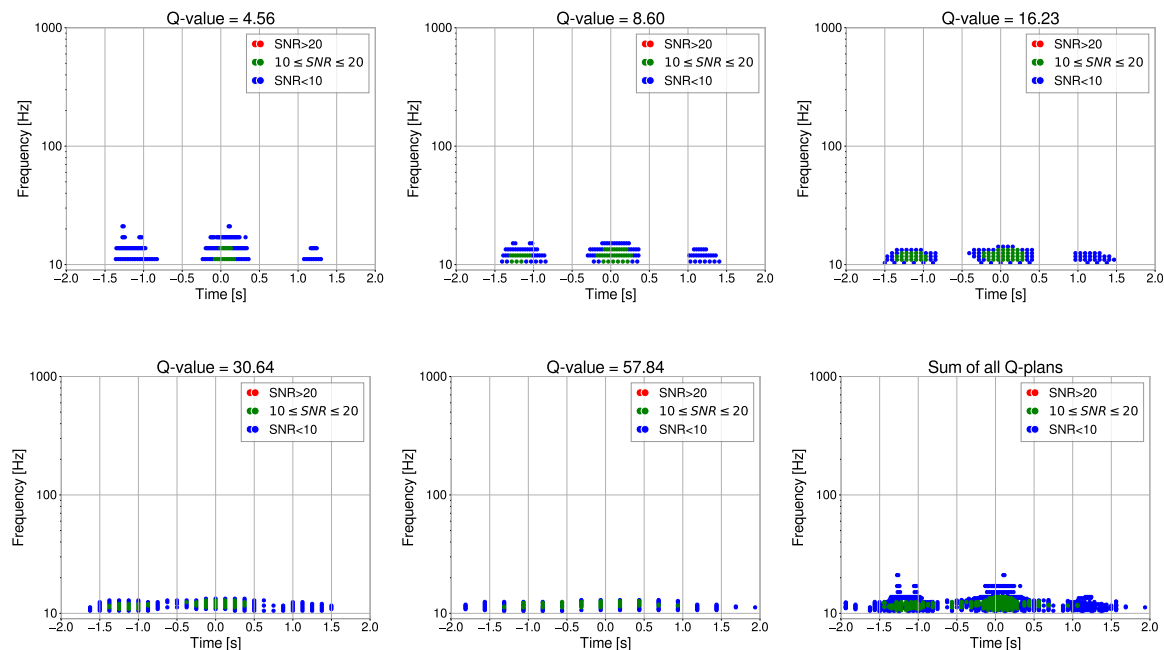


Figure 2: Unclustered Omicron triggers during a low-frequency glitch at LLO. The first to fifth images represent the same glitch at different Q-values, ranging from 4.56 to 57.84. This figure highlights how glitch morphology changes with varying Q-values. While we maintain good time resolution with Q-values ranging from 4 to 16, we begin to lose that for values higher than 30, transitioning towards more frequency resolution. The last image shows all Omicron triggers for various Q-values; it can be regarded as a sum of all other Q-planes.

For comparison, Figure 3 presents the spectrogram generated using the Q-transform via `GWpy` [28] for the same glitch at two different Q-values (8.60 and 57.84). This is one of the most common representations of transient signals in the detector’s data. On the left side, with a low Q-value, three repeating arches over time are visible, which is consistent with the first three images in Figure 2. On the right side, the high Q-value reveals a prominent line, similar to the fourth and fifth images in Figure 2.

Glitches from the same source usually have similar features, allowing patterns to be identified in the data and enabling the creation of glitch classes. These features include arch shapes, their repetitions, the morphology and the width of bands (whether narrow or broad), SNR, frequency range (whether low or high), and others. Gravity Spy is a successful tool that involves volunteers, machine-learning techniques, and Detchar

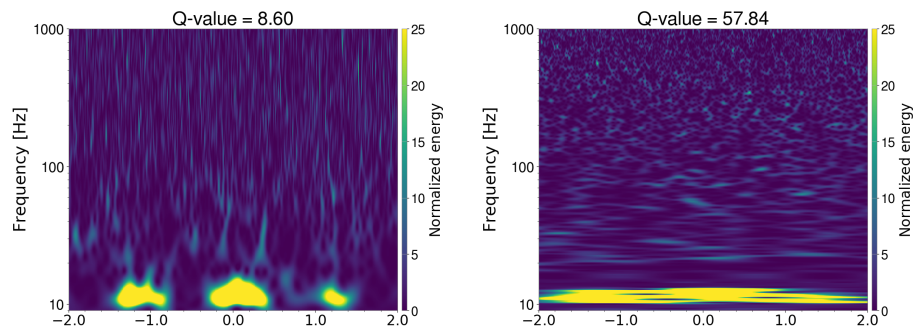


Figure 3: Spectrograms of different Q-values generated with GWpy for the same glitch presented in Figure 2. This illustrates the impact of differing Q-values on glitch morphology.

experts for classifying glitches [22]. The names of the classes are derived either from the shapes observed in the images or from prior knowledge of their sources. Examples include *Tomte*, *Low Frequency Burst*, *Blip*, *Scattered Light*, and *Extremely Loud*, among others. Figure 4 presents spectrograms illustrating selected glitch classes observed during O3b at LLO. Further details on glitch classifications can be found in [22,23,29,30].

To classify glitches, tools like Gravity Spy rely on Omicron’s clustered information. Whenever Omicron detects a glitch, these tools generate one or more images similar to Figure 4 and classify them accordingly. This paper analyzes glitches based on their morphologies derived from unclustered Omicron data using all Q-values, as shown in the last image in Figure 2, enabling computationally efficient and rapid analysis without requiring the reapplication of the Q-transform or the creation of images as a training dataset.

The t-SNE (t-distributed stochastic neighbor embedding) algorithm is a statistical technique that allows visualization of high-dimensional data points in a lower-dimensional space [34], typically two or three, which aligns with human visual perception capabilities. In addition to dimensionality reduction, the algorithm applies a clustering based on the similarities between pairwise data points, giving an extra interpretation possibility for complex data sets. In the context of glitch analysis, this unsupervised technique has been applied in various ways, including visualizing the Gravity Spy dataset using lower-resolution spectrograms [35], examining compression through autoencoders for anomaly detection in LIGO’s glitch populations [36], and comparing results before and after modifications, such as improving interpretability using weights derived from attention modules, which were proposed and implemented as part of Gravity Spy during O4 [37].

This study focuses on applying t-SNE to morphologies derived from unclustered Omicron triggers, which have proven effective in identifying glitch classes in the gravitational wave data channel [38]. This approach removes the need to create image datasets, significantly accelerating algorithmic analysis. Another important aspect is that this analysis can be conducted independently, without prior knowledge of glitch

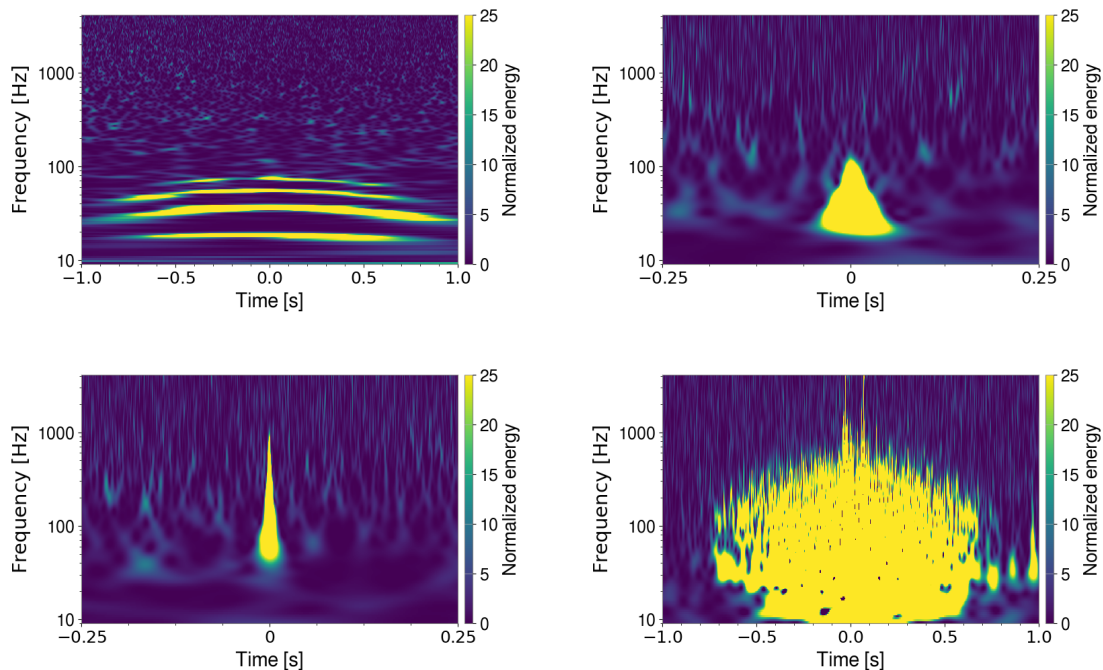


Figure 4: Spectrograms of four different classes of glitches selected during O3b at LLO: (Top left) *Scattered Light*, although many times these glitches are known to be caused by stray light, the main goal is to identify the surface that is scattering the light. (Top right) *Tomte*, observed during ESD bias voltage ramping [31], with their exact causes still unknown. (Bottom left) *Blip*, a class of glitches with no identified sources. (Bottom right) *Extremely Loud*, typically characterized by a very high SNR (greater than 100). Recent data suggest these glitches may be associated with scattered light near the End Test Mass (ETM) [32, 33].

classes. In the following section, we begin by using the Gravity Spy classes as a reference to investigate how glitch duration, SNR normalization, and the exclusive use of either low or high Q-values influence the results.

3. *t*-SNE Applied to LLO Glitches During O3b with Prior Knowledge of Classes

We selected a dataset of 1,000 random glitches from each of the ten most common Gravity Spy classes in O3b (with a minimum of 90% confidence in each glitch’s classification). A representation, as shown in the last image of Figure 2, was built using all Q-values. Each image was then divided into 30×41 pixels that could include zero, one, or more omicron triggers. Each pixel stored the value of the trigger with the highest SNR. Using this data, a matrix was created for each transient, which was then flattened into a data vector of 1,230 elements. This approach is similar to the one discussed in [38]. However, it differs by using shorter-duration intervals in the creation of glitch morphology, higher time resolution, and normalized SNR values. More details

will be discussed in the following sections.

Figure 5 presents a scatter plot of the two t-SNE output coordinates applied to this dataset, where each color represents a different Gravity Spy class. In general, the groups are well-clustered. The class *Low Frequency Lines* (in pink) is now divided into two distinct subgroups: one located on the right side, corresponding to frequencies around 20 Hz, and another at the center bottom, corresponding to frequencies around 12 Hz and 13 Hz. Additionally, a small group exists between this last subgroup and the *Low Frequency Burst* class (in brown), with a frequency around 11 Hz. These distinctions observed through t-SNE are attributable to the frequency resolution used in constructing the dataset. Additionally, there is a small subdivision within the *Fast Scattering* class, depicted in red. The frequencies between these subdivisions differ as well, with the lower subdivision exhibiting frequencies around 27 Hz, while the upper subdivision displays frequencies near 39 Hz.

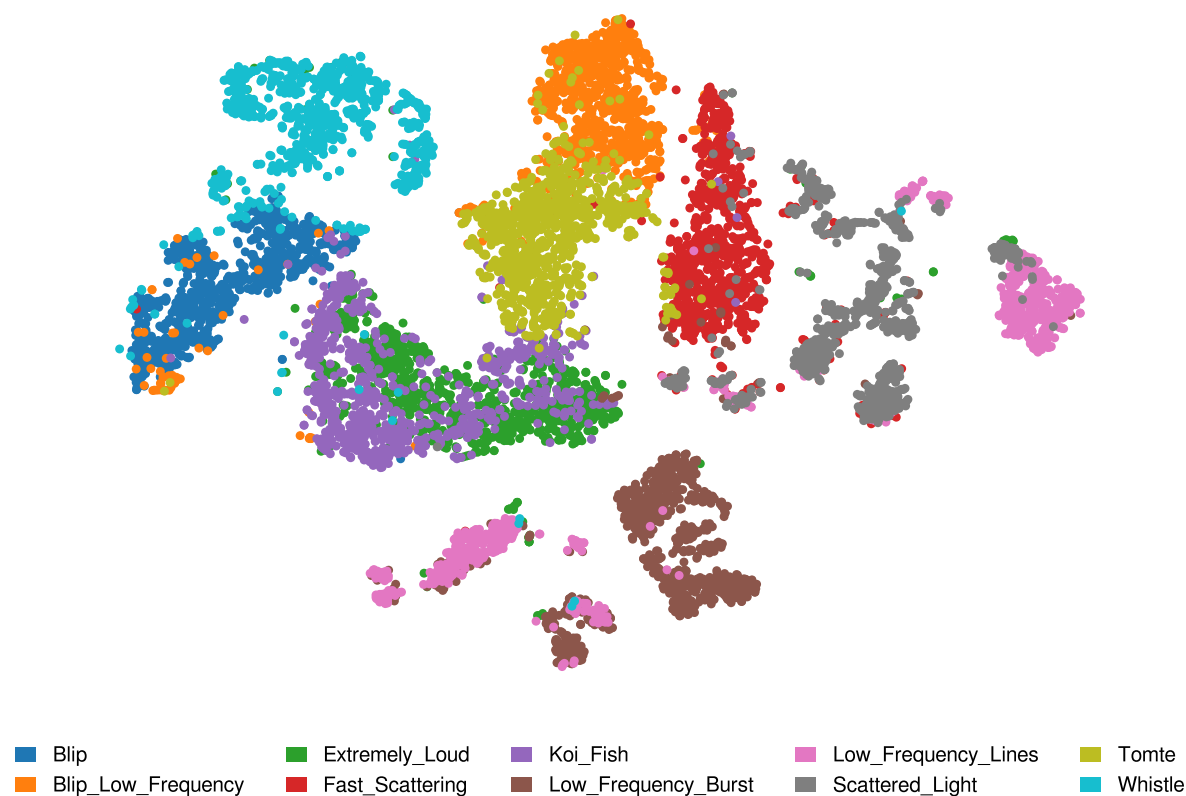


Figure 5: Scatter plot of t-SNE coordinates representing 10,000 data points from a 1,230-dimensional space derived from unclustered Omicron triggers. Each point represents a glitch, with colors indicating the classification according to Gravity Spy. The input data included triggers from all Q-planes, as depicted in the last image of Figure 2.

There is a significant overlap between *Koi Fish* (purple) and *Extremely Loud* (green) classes. Figure 6 shows two data matrices used as input from unclustered Omicron files, with a glitch classified as *Extremely Loud* on the left side and *Koi Fish* on the

right. Indeed, some of them are morphologically very similar and the main feature that differentiates them is the SNR, as will be shown in subsection 3.2; further details about their similarities are also discussed in [39]. Another important aspect to mention is that the *Scattered Light* class was subdivided into smaller groups. This subdivision occurred because the technique is sensitive to variations in the duration of the arches, the number of arches, and the peak frequency.

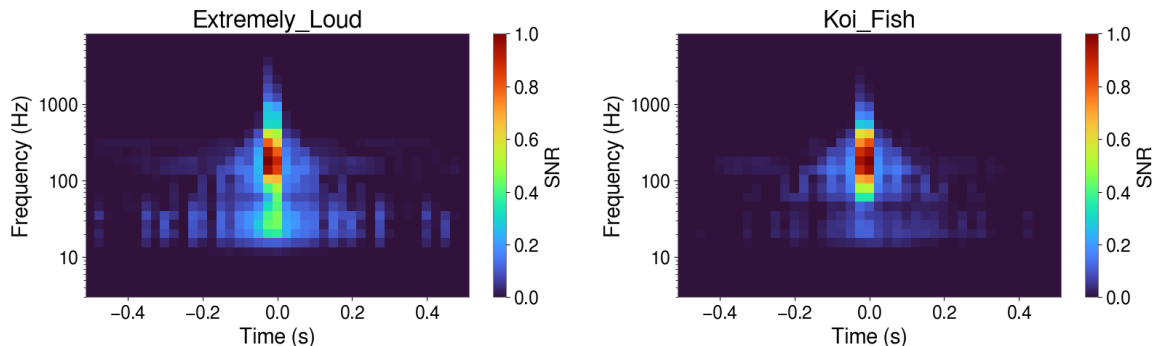


Figure 6: Two data matrices were used as input to *t*-SNE. The left matrix was classified as *Extremely Loud*, and the right as *Koi Fish*. The normalization in SNR shows that their morphologies are quite similar, which explains the overlaps from *t*-SNE output.

3.1. Influence of window duration:

When a glitch is centered at time t and a window duration w is selected, triggers are sought within the time interval $t - w/2$ to $t + w/2$. The current primary classification method used in LIGO data, Gravity Spy, employs four different image windows to classify each glitch: 0.5 s, 1.0 s, 2.0 s, and 4.0 s [22, 37], allowing for large-scale analysis as well as examination of finer details. The first image in Figure 7 presents the *t*-SNE output when we use $w = 4.0$ s. Although it’s still possible to see clusters of colors, there are more overlaps than before in Figure 5, where a window duration of $w = 1.0$ s is used. This increased overlap occurs because longer durations make it more difficult to distinguish short-duration glitches, effectively causing a “zoom out” effect on the morphological features, which explains why *Blip*, *Koi Fish*, and *Extremely Loud* glitches appear closer together. Although shorter durations provide clearer distinctions between some classes, we opt for keeping $w = 1.0$ s, which allows us to observe arches (as shown in Figure 4), but not necessarily the repetition of them.

3.2. Influence of SNR

The proposed method exhibits sensitivity to the normalization of the data vectors. The top-right image in Figure 7 presents the same analysis performed without normalizing SNR values. This lack of normalization can assist in identifying outliers and stronger

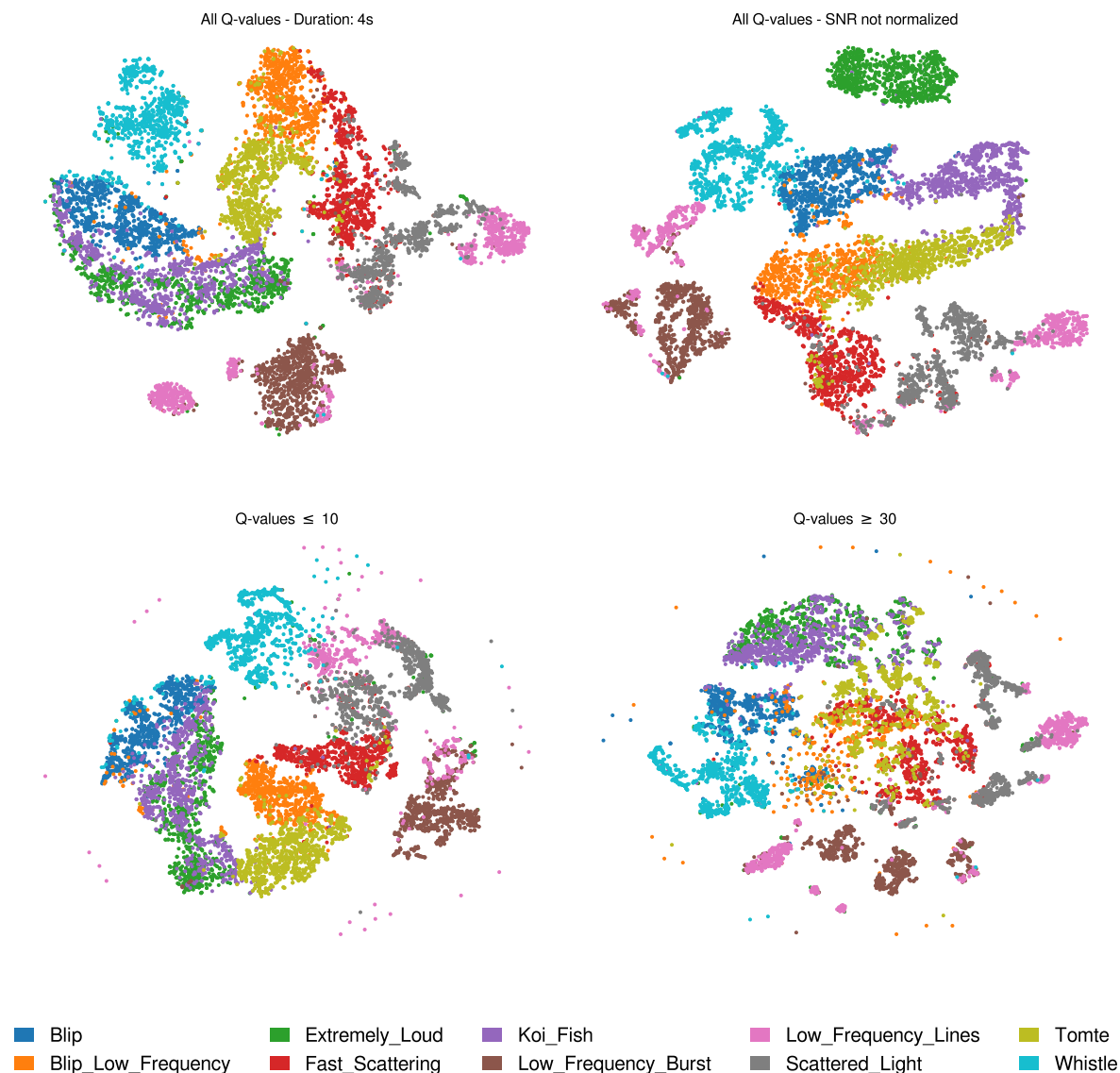


Figure 7: Effects on the *t*-SNE output for the same dataset used to create Figure 5, with small changes in the input parameters. Top left: 4-second window, instead of a 1-second window. Although groups of colors are visible, they are more interconnected. Top right: same dataset (with 1-second window) using non-normalized SNR. The *Extremely Loud* class (green) stands out due to its high SNR, resulting in an isolated cluster, while other classes appear more interconnected. Bottom: This application illustrates the impact of Q-values. The left image shows a dataset constructed from unclustered Omicron files, filtered to include only Q-values less than 10. In contrast, the right image displays triggers with Q-values greater than 30. In this dataset, high Q-values affect the analysis more, leading to more overlaps in the center. However, each range of Q-values can be selected according to specific interests, such as achieving better resolution in time or frequency.

glitches in the dataset. However, as morphology is prioritized as the primary distinguishing feature among classes in this study, we utilize normalized data as a reference. In the unnormalized application, the *Extremely Loud* class is now distinctly isolated and no longer mixed with *Koi Fish* class, unlike the observation in Figure 5. Although some well-defined clusters are still observable, a drawback of this approach is that the well-positioned cluster tends to “repel” other groups, making them appear more interconnected. This results in a division between regions with high SNR glitches (comprised solely of *Extremely Loud* in this case) and those with lower SNR glitches (containing all remaining classes).

3.3. Influence of *Q*-Values

The *Q*-value is intrinsically linked to the time and frequency resolutions of the glitch spectrogram. This relationship implies that, in certain cases, the choice of *Q*-value can significantly influence the morphology of the glitch, as demonstrated in Figures 2 and 3. During the O4a run, LHO was notably impacted by glitches in the broadband frequency range from 20 to 40 Hz [18] (as also presented in Figure 1). Examination of their spectrograms revealed that, without specifying a *Q*-value, some glitches exhibited repeated patterns, as illustrated in the first image of Figure 8, while others displayed horizontal lines, as shown in the bottom-left image. Although they may initially appear different, these glitches have been identified as originating from the same source [40–42]; the difference in the morphologies is due to the varying *Q*-values.

Figure 7 illustrates the impact of *Q*-values on *t*-SNE clustering. The bottom left side of the figure shows the results when morphologies are derived using low *Q*-values (below 10), while the right side presents the results based on high *Q*-values (greater than 30). Both scenarios are affected by outliers on the edges, forming a circular arrangement. The output using high *Q*-values exhibits more overlaps in the central region among different classes and also results in some classes being subdivided into additional subclasses, as for the *Low Frequency Burst* (in brown), which reveals classes with different frequencies. Here, we highlight a potential application of this technique: selecting the *Q*-value range according to specific interests. For instance, we can study a single class with high *Q*-values to explore possible subclasses - like the distinct frequencies seen in *Low Frequency Burst* - or focus on low *Q*-values to analyze longer durations and detect repetition over time.

In our approach, we do not select a single optimal *Q*-value; instead, we utilize all available *Q*-values. This comprehensive approach enables us to capture all relevant information. While this method does incorporate the limitations associated with varying resolutions in time and frequency, glitches originating from the same source will be similarly affected, resulting in comparable morphologies. This consistency is beneficial compared to selecting only one *Q*-value, which may not always capture the full range of morphological features.

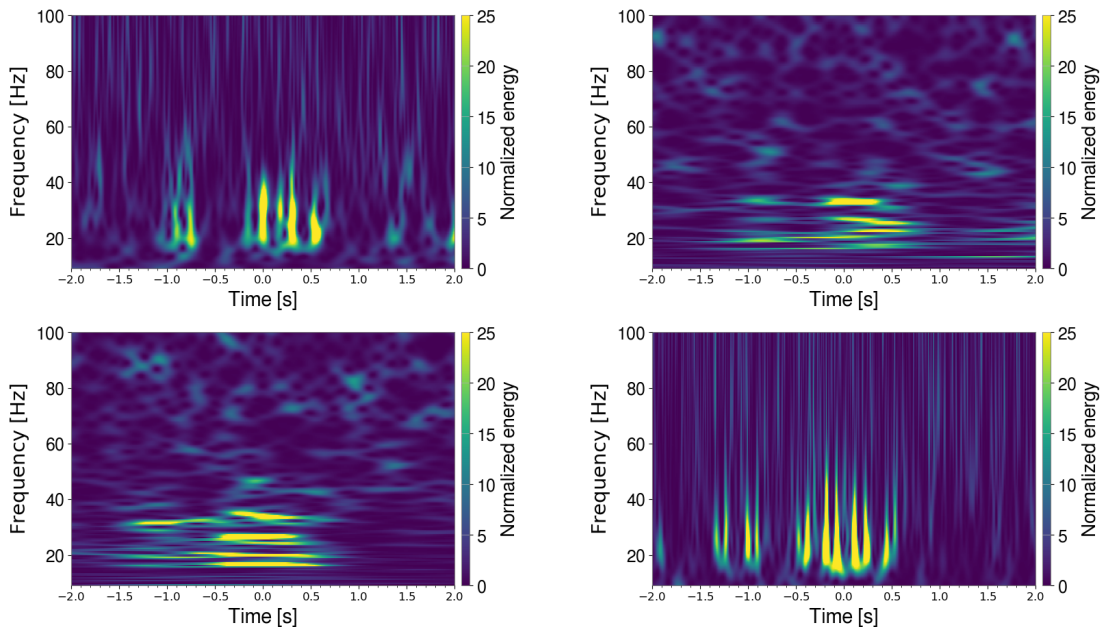


Figure 8: Visualization of glitches in the broadband frequency range from 20 to 40 Hz at LHO during the O4a run. The spectrograms show glitches that appear distinct (top-left and bottom-left) but actually originate from the same source. Their respective spectrograms with different Q-values (top-right and bottom-right) illustrate how the choice of Q-value can influence glitch morphology and potentially lead to misclassification and/or misinterpretations.

3.4. Applying a classifier

Supervised machine learning techniques typically require a training dataset to predict the class of a new glitch. While these methods can perform very well, building an effective training dataset presents challenges, especially when new data classes, such as previously unknown glitches, may emerge. The previous study by [38] proposes a classification approach based on the Support Vector Machine technique [43], which learns from previously labeled data. Here, we present an alternative method for glitch classification that is entirely independent of prior knowledge about the classes or their number.

The approach involves determining the number of clusters from the t-SNE output and assigning classes based on its two-dimensional representation. To achieve this, we applied **Agglomerative Clustering**, a hierarchical clustering method that assigns classes to datasets [44]. The algorithm begins by considering each data point as an individual cluster and iteratively merges pairs of clusters into a single cluster based on the configuration that minimizes the variance, calculated using Euclidean distance; this approach is also referred to as Ward’s method [45, 46]. This merging process continues until a stopping criterion is reached, which, in our case, is determined by evaluating different numbers of clusters using the **Silhouette Score** [47]. Both methods were

implemented using the Python library `Scikit-learn` [48].

The Silhouette Score evaluates the quality of the cluster configuration. For each data point i , it calculates the mean (Euclidean) distance a between i and all other data points in the same cluster, as well as the distance b between i and data points from the nearest cluster. The score $s(i)$ is given by

$$s(i) = \frac{b(i) - a(i)}{\max(a(i), b(i))}. \quad (2)$$

The score ranges from -1 to 1, where a value of 1 indicates the best configuration. Finally, the mean of the scores is calculated. This process was applied to the t-SNE output for a range of cluster numbers from 2 to 30. The optimal number of clusters was then selected based on the highest mean Silhouette Score, indicating the best fit for the output data. Figure 9 presents the t-SNE output, colored according to this classification method.

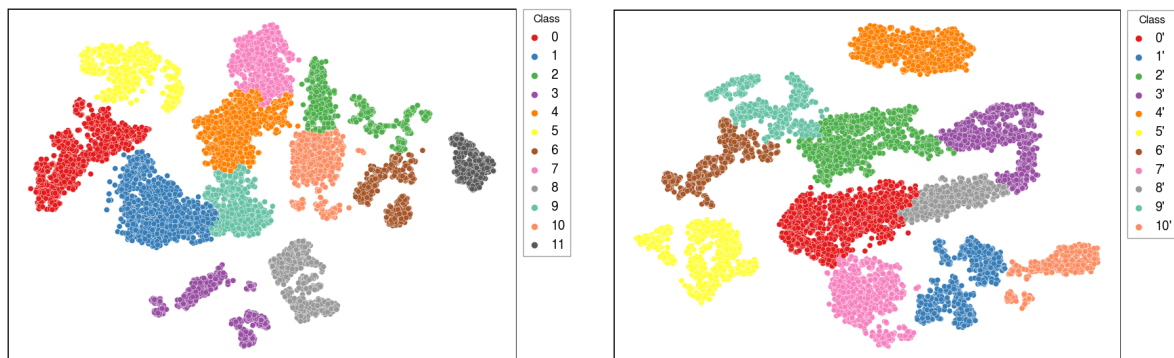


Figure 9: The same t-SNE output colored according to the classifier for normalized data, on the left, and not normalized, on the right. For comparisons with Gravity Spy classes, refer to Figure 5 and the second image in Figure 7, respectively.

The left side of Figure 9 presents the twelve identified classes labeled from 0 to 11. In comparison to Figure 5 and the Gravity Spy classes, our method identified two additional groups. One of these, depicted in purple as ‘Class 3’, corresponds to glitches classified as *Low Frequency Lines* and *Low Frequency Burst*. As discussed in Section 3, new groups were anticipated due to the sensitivity of t-SNE to different frequency ranges. This emphasizes that frequency resolution can be adjusted according to specific interests as well. Here, we are interested in presenting groups with differing peak frequencies, as they may originate from distinct sources.

The second new class, shown in green and designated as ‘Class 2’, differentiates between glitches within the scattering categories. This class includes glitches classified as *Fast Scattering* by Gravity Spy (indicated in red in Figure 5) and *Scattered Light* (in gray). Analysis of several spectrograms revealed that while these instances do not display similar morphology, all have higher frequencies compared to those in the primary clusters.

The right side of Figure 9 presents the results obtained without normalizing SNR, as illustrated in the top-right image of Figure 7. In this case, since most glitches are more interconnected due to loud glitches, close proximities may increase classification errors. However, the class labels generally align with Gravity Spy in both cases, indicating that data normalization can be applied based on specific analysis goals.

After determining the optimal number of classes and their distribution, we developed a classification method for new glitches. A representative vector was generated for each class using the 1,230 dimensions from unclustered Omicron data: 80% of each group’s data was used to compute the mean vector, while the remaining 20% served as a test dataset. To classify an ‘unknown’ glitch, we calculated the Euclidean distance between its vector and each class’s representative vector in high-dimensional space (since, in principle, the unknown glitches lack *t*-SNE coordinates). The class with the closest distance was assigned to the glitch. Figure 10 presents the classification results for the 20% of data reserved as the test dataset, with predicted labels (horizontal axis) compared to true labels (vertical axis).

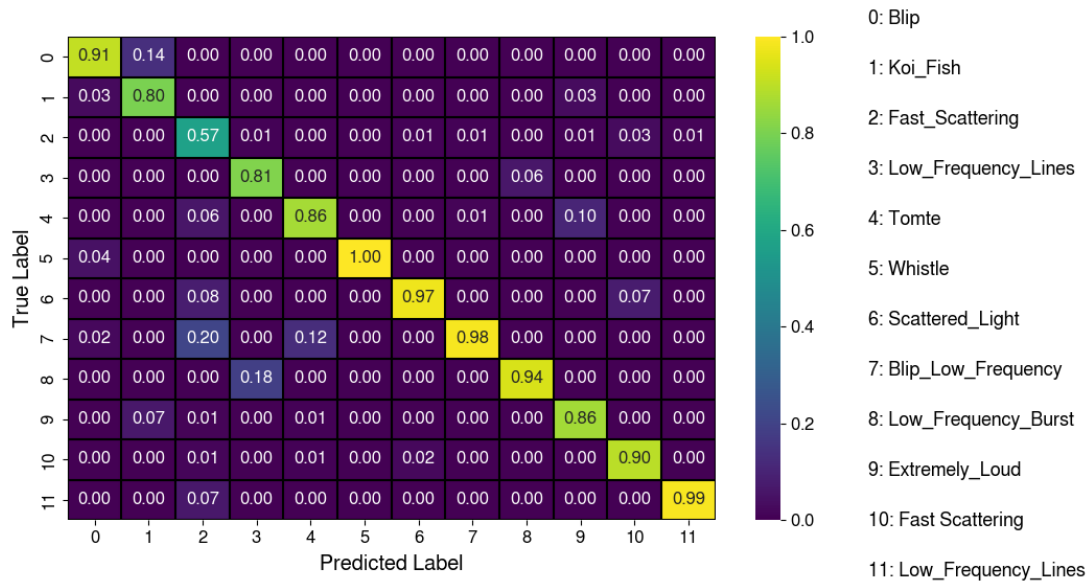


Figure 10: Confusion matrix illustrating glitch classification, employing Euclidean distance to determine the closest representative vectors from each class; the green and yellow cells signify a high degree of accuracy in predictions. On the right side, a list of correspondences to Gravity Spy classes is provided.

As indicated by the green and yellow regions, most glitches were classified correctly. On the right, a list of corresponding Gravity Spy classes for each identified class is provided. The only class with lower classification accuracy was ‘Class 2’, corresponding to the *Fast Scattering* class, which contained the subdivision mentioned previously. The total accuracy for the normalized dataset, calculated as the sum of diagonal elements divided by the matrix total, is 88.33%.

4. t-SNE Applied to LLO Glitches During O3b without Prior Knowledge of Classes

In this part of the analysis, we do not incorporate prior knowledge of glitch classifications. We randomly selected 2,000 clustered Omicron transients per month during the O3b at LLO (from November 2019 to March 2020), filtering glitch frequencies between 10 and 2048 Hz, with a minimum SNR of 7.5. We then applied t-SNE on these 10,000 noise transients using unclustered Omicron information for each, normalized SNR, a window duration of 1 second, and triggers for all Q-values. The resulting output is illustrated on the left side of Figure 11.

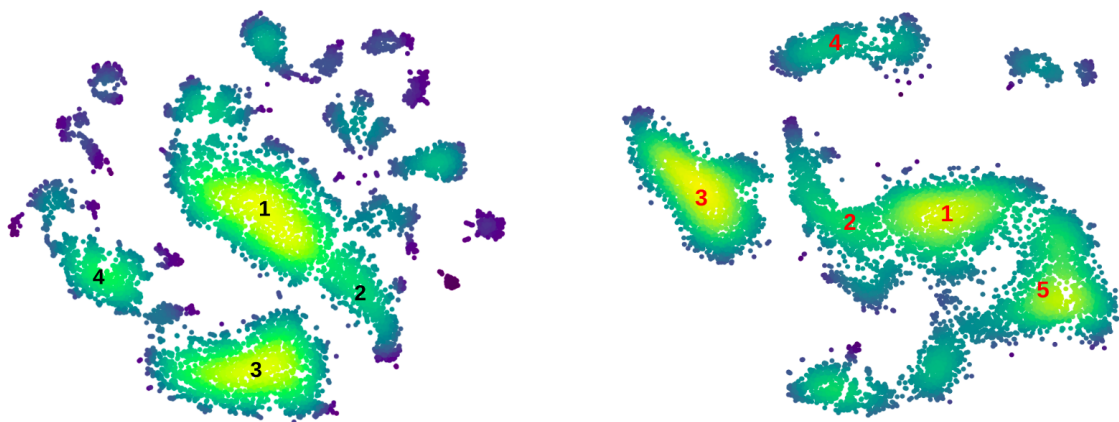


Figure 11: Application of t-SNE to O3b LLO data without using class information. The left side displays the output for 2,000 glitches selected from each month, with yellow indicating areas of higher data point density. The right side shows the output for 10,000 random transients selected without filtering by month.

There are four main large groups and many other smaller ones. We analyzed the four main groups, which give the most common classes of glitches during O3b. Group 1, the largest, consists of the *Fast Scattering* class with a frequency around 27 Hz, which corresponds to the lower part of the red color in Figure 5. Group 2 also follows a similar distribution and is equivalent to the *Fast Scattering* class. It exhibits the same characteristics in the upper part of the red color and it is in one of the new groups our method identified, with a higher frequency of approximately 39 Hz. Group 3 is primarily composed of *Tomte*, with *Blip Low Frequency* on the right side. Finally, group 4 comprises glitches equivalent to *Koi Fish* and *Extremely Loud*. Overall, they follow the same characteristics as observed in Figure 5.

When considering glitches throughout the entire O3b, the *Scattered Light* class was also among the most common glitch classes. However, our Omicron sample consisted of 2,000 observations per month and *Scattered Light* class was concentrated in only some months. After the implementation of RC tracking [12] in January 2020, the number of glitches associated with this class decreased significantly, which explains the absence of a corresponding large cluster in the t-SNE output. Nevertheless, this class still appeared

within the smaller groups in the upper right corner of the image. As mentioned earlier, each small group exhibits distinct characteristics, including varying durations, numbers of harmonics, and differences in the arches.

If we select 10,000 glitches randomly during all O3b, without filtering by month, this class, being one of the most common, becomes more prominent, as shown in the right side of Figure 11 in the region labeled 5 (in red). This entire region and the lower left area contain *Scattered Light* glitches, which are more concentrated than in the previous case. Each number in this new configuration corresponds to the groups on the left side; for example, number three in both cases includes more glitches classified as *Tomte*. Since we are selecting random data, the most common classes will naturally be predominant. Selecting an equal number per month allows, for instance, an analysis of glitch behavior over time monthly, providing insights into when each group appears more frequently. An example of tracking glitches over one week is provided in the following section.

5. Analysis for One Week During O4a: Searching for Outliers

An advantage of this approach lies in its ability to analyze data with low latency and track changes over time. To verify this capability, we selected a week during O4a, specifically from September 3rd to September 8th, to investigate daily behavior without prior knowledge of the glitch classes. This allowed us to assess the natural occurrence and progression of glitches throughout the week. Figure 12 shows the application of *t-SNE* to the dataset, illustrating how the data evolves over the period from September 3rd to September 8th.

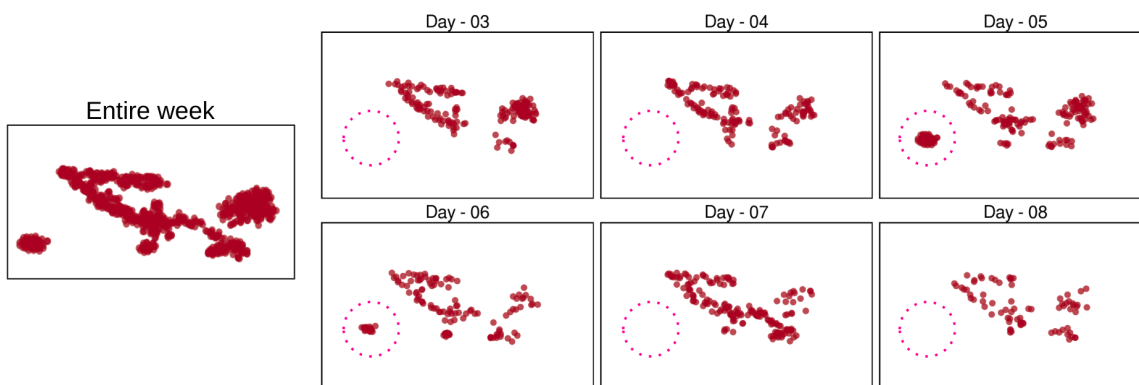


Figure 12: *t-SNE* visualization of data from September 3rd to 8th, 2024. On the left, the output for the entire week is presented, while on the right, the data is shown day by day, highlighting the formation and disappearance of a cluster (within the dashed circle).

The first image (on the left side) in Figure 12 presents the output for the entire week, followed by the behavior observed on each day. Notably, a distinct cluster emerges

on the left side of the plot after September 5th (highlighted by the dashed circle), shrinks on September 6th, and disappears by September 7th. This behavior suggests a temporal pattern linked to specific physical changes in the system. These glitches, observed at a frequency of 60 Hz, were attributed to voltage bias changes in the electrostatic drive of the End Test Mass Y (ETMY) arm, as detailed in [49]. This analysis demonstrates the potential to track temporal variations and associate them with environmental or instrumental conditions. The method can be applied on various timescales, including weekly, monthly, daily, or even hourly, depending on the specific objectives.

6. Conclusions and Future Applications

This paper presents a method for studying non-Gaussian noise transients (glitches) in gravitational wave detector data, focusing on the LIGO Livingston observatory through the examination of Omicron data. We employ clustering and classification techniques and investigate how variations in parameters influence the analysis. Since the primary dataset relies solely on unclustered Omicron information, the processes of time series acquisition, Fourier or Q-transforms for generating spectrograms, as well as the development of a training dataset, are not required. While supervised machine learning methods can yield improved classifications, establishing a robust training dataset poses significant challenges, often necessitating extensive time and frequent retraining to accommodate new classes.

We utilized the t-SNE algorithm, a technique designed to visualize high-dimensional data in reduced dimensions by clustering data based on similarities, specifically applied to the normalized Omicron data during O3b. In our initial application during O3b, we demonstrated that the most common classes were well grouped, except *Koi Fish* and *Extremely Loud* glitches. These two classes were identified as having similar morphologies, primarily differentiated by their SNR values, which significantly impact the results. When normalized SNR is not employed as input data, the *Extremely Loud* class emerges as an outlier. Here, we chose to utilize normalized data to focus solely on glitch morphologies. If two glitches exhibit similar morphologies, they may originate from the same source, making it beneficial to group them together rather than separating them solely based on differences in SNR. However, the choice of approach should be guided by the primary objectives of the research.

We also conducted a study of the duration of the glitches, leading us to choose a window of 1 s, which is large enough to retain information from classes such as *Scattered Light* while being short enough to avoid mixing similar classes. This parameter is adjustable and, for instance, a longer window could be employed to study the repetition of scatter arches alongside low Q-values derived from the Q-transform, which allows for better temporal resolution. Our comparison of Q-values highlights how their variation affects the glitch morphology and the visualization in the t-SNE embedding. Higher Q-values (greater than 30), which provide poorer temporal resolution, demonstrate significant overlap among *Tomte*, *Fast Scattering*, and *Blip Low Frequency*. In this

context, distinct small clusters were identified for *Low Frequency Burst*, which exhibited slight differences in frequency. This highlights a key feature of our methodology: the ability to select the range of Q-values based on the researcher’s interests. In our approach here, we utilized all Q-values, effectively summing all Q-planes from Omicron. This method captures triggers with lower resolution in time and frequency, but does so across all noise transients, ensuring that glitches with similar features are affected similarly.

Additionally, we implemented a classifier based on the minimum Euclidean distance between an unknown glitch and the representative vectors created for each class obtained from the t-SNE output. The classifier was also applied to the same O3b data and identified two additional classes compared to Gravity Spy when the data were normalized, and one additional class when they were not. The main distinction arose between low-frequency glitches that differed in frequency, with one group centered around 12 Hz.

We also explored the method applied to O3b without prior knowledge of glitch classifications, and we observed similar behaviors compared to the case with prior knowledge, particularly due to the shapes of the most common glitches. One of the main objectives of this method is to present a means of tracking glitches over time and relating them to potential causes and sources. In this regard, we conducted a week-long analysis to identify outliers in the data. By analyzing day by day, we observed a cluster of glitches shrinking, which were associated with instrumentation changes.

In conclusion, we present characteristics of an alternative approach to analyzing glitches, particularly in low-latency scenarios (relying on Omicron), by leveraging Omicron for rapid insights into glitch behavior. Although this method may not provide the highest resolution for classifying glitches, it facilitates a temporal understanding of glitch behavior, aiding in source identification. Furthermore, it eliminates the need to create a training dataset. Future work may explore advanced machine learning techniques to further refine glitch classification and mitigation strategies, including the use of multiple data matrices to study glitches, testing with different durations, and varying Q-value ranges.

Acknowledgments

We would like to thank Jane Glanzer for the comments and suggestions. We express our gratitude to the members of the LIGO Detector Characterization Group and the LIGO-Virgo-KAGRA (LVK) collaboration for their valuable discussions. This work was supported by the National Science Foundation under grant number NSF-PHY2110509. The material is based upon work supported by NSF’s LIGO Laboratory, a major facility fully funded by the National Science Foundation. Additionally, the work utilizes the LIGO computing clusters and data from the Advanced LIGO detectors; the authors are grateful for the computational resources provided by the LIGO Laboratory, supported by National Science Foundation Grants PHY-0757058 and PHY-0823459.

References

- [1] Abbott B P, Abbott R, Abbott T, Abraham S, Acernese F, Ackley K, Adams C, Adhikari R, Adya V, Affeldt C *et al.* 2019 *Physical Review X* **9** 031040
- [2] Abbott R, Abbott T, Acernese F, Ackley K, Adams C, Adhikari N, Adhikari R, Adya V, Affeldt C, Agarwal D *et al.* 2023 *Physical Review X* **13** 041039
- [3] Abbott R, Abbott T, Acernese F, Ackley K, Adams C, Adhikari N, Adhikari R, Adya V, Affeldt C, Agarwal D *et al.* 2024 *Physical Review D* **109** 022001
- [4] Collaboration L *LIGO/Virgo/KAGRA Public Alerts* <https://gracedb.ligo.org/superevents/public/04a/>
- [5] Aasi J, Abbott B, Abbott R, Abbott T, Abernathy M, Ackley K, Adams C, Adams T, Addesso P, Adhikari R *et al.* 2015 *Classical and quantum gravity* **32** 074001
- [6] Harry G M (LIGO Scientific) 2010 *Class. Quant. Grav.* **27** 084006
- [7] Martynov D V, Hall E, Abbott B, Abbott R, Abbott T, Adams C, Adhikari R, Anderson R, Anderson S, Arai K *et al.* 2016 *Physical Review D* **93** 112004
- [8] Acernese F, Agathos M, Agatsuma K, Aisa D, Allemandou N, Allocca A, Amarni J, Astone P, Balestri G, Ballardín G *et al.* 2014 *Classical and Quantum Gravity* **32** 024001
- [9] Akutsu T, Ando M, Arai K, Arai Y, Araki S, Araya A, Aritomi N, Aso Y, Bae S, Bae Y *et al.* 2021 *Progress of Theoretical and Experimental Physics* **2021** 05A101
- [10] Akutsu T, Ando M, Arai K, Arai Y, Araki S, Araya A, Aritomi N, Asada H, Aso Y, Atsuta S *et al.* 2019 *NATURE ASTRONOMY* **3** 35–40
- [11] Aso Y, Michimura Y, Somiya K, Ando M, Miyakawa O, Sekiguchi T, Tatsumi D, Yamamoto H and Collaboration) K 2013 *Physical Review D—Particles, Fields, Gravitation, and Cosmology* **88** 043007
- [12] Soni S, Austin C, Effler A, Schofield R, González G, Frolov V, Driggers J C, Pele A, Urban A, Valdes G *et al.* 2020 *Classical and Quantum Gravity* **38** 025016
- [13] Soni S, Glanzer J, Effler A, Frolov V, González G, Pele A and Schofield R 2024 *Classical and Quantum Gravity* **41** 135015
- [14] Abbott R, Abbott T D, Acernese F, Ackley K, Adams C, Adhikari N, Adhikari R X, Adya V, Affeldt C, Agarwal D *et al.* 2021 *Physical Review D* **104** 122004
- [15] Abbott B P, Abbott R, Abbott T, Acernese F, Ackley K, Adams C, Adams T, Addesso P, Adhikari R X, Adya V B *et al.* 2017 *Physical review letters* **119** 161101
- [16] Davis D, Areeda J S, Berger B K, Bruntz R, Effler A, Essick R, Fisher R, Godwin P, Goetz E, Helmling-Cornell A *et al.* 2021 *Classical and Quantum Gravity* **38** 135014
- [17] Acernese F, Agathos M, Ain A, Albanesi S, Allocca A, Amato A, Andrade T, Andres N, Andrés-Carcasona M, Andrić T *et al.* 2023 *Classical and Quantum Gravity* **40** 185006
- [18] Soni S, Berger B, Davis D, Renzo F D, Effler A, Ferreira T, Glanzer J, Goetz E, González G, Helmling-Cornell A *et al.* 2024 *arXiv preprint arXiv:2409.02831*
- [19] Robinet F, Arnaud N, Leroy N, Lundgren A, Macleod D and McIver J 2020 *SoftwareX* **12** 100620
- [20] Robinet F *GWOLLUM* <https://virgo.in2p3.fr/GWOLLUM/v2r2/index.html?Main/convention.html>
- [21] Brown J C 1991 *The Journal of the Acoustical Society of America* **89** 425–434
- [22] Zevin M, Coughlin S, Bahaadini S, Besler E, Rohani N, Allen S, Cabero M, Crowston K, Katsaggelos A K, Larson S L *et al.* 2017 *Classical and quantum gravity* **34** 064003
- [23] Glanzer J, Banagiri S, Coughlin S, Soni S, Zevin M, Berry C P L, Patane O, Bahaadini S, Rohani N, Crowston K *et al.* 2023 *Classical and Quantum Gravity* **40** 065004
- [24] Zevin M, Jackson C B, Doctor Z, Wu Y, Østerlund C, Johnson L C, Berry C P, Crowston K, Coughlin S B, Kalogera V *et al.* 2024 *The European Physical Journal Plus* **139** 100
- [25] Chatterji S K 2005 *The search for gravitational wave bursts in data from the second LIGO science run* Ph.D. thesis Massachusetts Institute of Technology
- [26] Robinet F 2016 Omicron: an algorithm to detect and characterize transient events in gravitational-

- wave detectors
- [27] Gabor D 1946 *Journal of the Institution of Electrical Engineers-part III: radio and communication engineering* **93** 429–441
 - [28] Macleod D, Urban A, Coughlin S, Massinger T, Pitkin M, George R, Altin P, Areeda J, Singer L, Quintero E, Leinweber K and Badger T 2020 gwpy/gwpy: 2.0.1 (v2.0.1) <https://doi.org/10.5281/zenodo.3973364>
 - [29] Zevin M *et al.* 2024 *Eur. Phys. J. Plus* **139** 100 (Preprint [2308.15530](https://arxiv.org/abs/2308.15530))
 - [30] Glanzer J, Banagari S, Coughlin S, Zevin M, Bahaadini S, Rohani N, Allen S, Berry C, Crowston K, Harandi M, Jackson C, Kalogera V, Katsaggelos A, Noroozi V, Osterlund C, Patane O, Smith J, Soni S and Trouille L *Gravity Spy Machine Learning Classifications of LIGO Glitches from Observing Runs O1, O2, O3a, and O3b* <https://doi.org/10.5281/zenodo.5649212>
 - [31] Buikema A, Davis D, Kulkarni S, Essick R and Massinger T *Glitches during ESD ramping resemble glitch class from O2* <https://alog.ligo-la.caltech.edu/aLOG/index.php?callRep=42851>
 - [32] Ferreira T and Gonzalez G *Analysis of Individual TR ERM PDs During Loud Glitches* <https://alog.ligo-la.caltech.edu/aLOG/index.php?callRep=73447>
 - [33] Frolov V *Scattered light in the arms making large DARM glitches* <https://alog.ligo-la.caltech.edu/aLOG/index.php?callRep=72968>
 - [34] Van der Maaten L and Hinton G 2008 *Journal of machine learning research* **9**
 - [35] Bahaadini S, Noroozi V, Rohani N, Coughlin S, Zevin M, Smith J R, Kalogera V and Katsaggelos A 2018 *Information Sciences* **444** 172–186
 - [36] Laguarda P, van der Laag R, Lopez M, Dooney T, Miller A L, Schmidt S, Cavaglia M, Caudill S, Driessens K, Karel J *et al.* 2024 *Classical and Quantum Gravity* **41** 055004
 - [37] Wu Y, Zevin M, Berry C P, Crowston K, Østerlund C, Doctor Z, Banagiri S, Jackson C B, Kalogera V and Katsaggelos A K 2024 *arXiv preprint arXiv:2401.12913*
 - [38] Ferreira T A and Costa C A 2022 *Classical and Quantum Gravity* **39** 165013
 - [39] Nichols S A 2024
 - [40] Vajente G *DARM bicoherence: evidence of non-stationary noise 10-50 Hz* <https://alog.ligo-wa.caltech.edu/aLOG/index.php?callRep=71005>
 - [41] Vajente G *DARM noise 20-40 Hz correlated with 2.6 Hz peak* <https://alog.ligo-wa.caltech.edu/aLOG/index.php?callRep=71092>
 - [42] Vajente G *Low frequency noise improved with new CHARD Y controller and reduced TM damping* <https://alog.ligo-wa.caltech.edu/aLOG/index.php?callRep=71927>
 - [43] Noble W S 2006 *Nature biotechnology* **24** 1565–1567
 - [44] Xu R and Wunsch D 2005 *IEEE Transactions on neural networks* **16** 645–678
 - [45] Ward Jr J H 1963 *Journal of the American statistical association* **58** 236–244
 - [46] Sharma S, Batra N *et al.* 2019 Comparative study of single linkage, complete linkage, and ward method of agglomerative clustering *2019 international conference on machine learning, big data, cloud and parallel computing (COMITCon)* (IEEE) pp 568–573
 - [47] Rousseeuw P J 1987 *Journal of computational and applied mathematics* **20** 53–65
 - [48] Pedregosa F, Varoquaux G, Gramfort A, Michel V, Thirion B, Grisel O, Blondel M, Prettenhofer P, Weiss R, Dubourg V *et al.* 2011 *the Journal of machine Learning research* **12** 2825–2830
 - [49] Betzwieser J *Running with ETMY ESD at 100V instead of -30V* <https://alog.ligo-la.caltech.edu/aLOG/index.php?callRep=67138>